Heterogeneous Ozonolysis of Cypermethrin Using Real-Time Monitoring FTIR Techniques

M. Segal-Rosenheimer and Y. Dubowski*

Department of Civil and Environmental Engineering, Technion − Israel Institute of Technology, Haifa 32000, Israel

Received: April 16, 2007; In Final Form: June 5, 2007

Cypermethrin is a synthetic pyrethroid that has become one of the most important insecticides in wide-scale use both indoors and outdoors. Although cypermethrin is likely to become adsorbed (following its application) on aerosols and upon stagnant outdoor and indoor surfaces, its atmospheric degradation processes are not well understood yet. Here, we have quantitatively investigated the oxidation of cypermethrin by gaseous ozone, including kinetic analysis and identification of volatile and nonvolatile products. The investigation was done using a novel apparatus, combining two FTIR setups for the parallel analysis of both condensed and gas phases. The nonintrusive analysis method enabled one to follow the reaction in real time without any alteration that may affect the process. The proposed reaction mechanism involves both an ozonide formation and an ester cleavage process that occur due to secondary radical chain reactions. It was found to follow a Langmuir−Hinshelwood mechanism with a half-life time of cypermethrin in relation to average atmospheric ozone level of 50 ppb of about 21 days. These results indicate that the heterogeneous oxidation of cypermethrin by ozone cannot be neglected in the overall environmental fate cycle for this material. Furthermore, several of the yielded condensed products are toxic and more polar than the parent molecule, a fact that makes them possible contaminators of groundwater in contrast to the parent molecule. Gaseous phosgene, a known nerve gas, was found to be generated during the ozonolysis reaction, which may increase the hazard in the use of cypermethrin as an indoor insecticide.

1. Introduction

Pesticides are highly toxic compounds that unlike other pollutants are intentionally introduced in large quantities to the environment. The vast majority of them are applied to agricultural lands, but they are also widely used in urban areas as herbicides, insecticides, and fungicides. Pesticides may be promoted into the atmosphere during their application via drift of aerosols, as well as by volatilization or dust erosion from treated surfaces after application.[1] Transport of airborne pesticides and their degradation products are likely to introduce them to nontarget and widespread areas.[2,3] Although previous studies indicate that a major portion of applied pesticides wind up in the atmosphere,[2,4−6] this is the medium about which we know the least regarding pesticides' fate.

During their presence on applied surfaces (indoor and outdoor) as well as during atmospheric transport (most likely adsorbed to aerosols), pesticides may react with reactive atmospheric species and/or solar radiation. These degradation reactions may yield products that differ from the parent molecule in their toxicity, stability, and their mobility in different mediums.[7] Thus, to better evaluate the environmental and health impacts of pesticides, it is crucial to understand also their interactions with the atmosphere.

Cypermethrin is a synthetic pyrethroid insecticide that has high insecticidal activity and low avian and mammalian toxicity.[8] It is widely used and is gaining popularity replacing the organophosphate (OP) insecticide family, mainly for orchards, vegetables, as an indoor insecticide, and as an outdoor mosquito control insecticide. As such, it is sprayed in large areas as ultralow volume liquid spray that releases very small aerosol droplets that stay longer in the air. Indeed, cypermethrin is less toxic to birds and mammals (LD_{50} of 200−10 000 mg/kg) in comparison to the OP pesticides' family, but it is very toxic to aquatic biota (LC_{50} 0.2−3 ppb).[9] Although cypermethrin is a low-vapor pressure insecticide (1.3×10^{-9} mmHg at 20 °C) and is not expected to be present in the gas phase, it is susceptible to reside in the atmosphere in its aerosolized form or adsorbed upon atmospheric aerosols.[10] In addition, following its application, cypermethrin will remain adsorbed upon stationary surfaces (soil, crops, buildings, etc) that are also exposed to atmospheric oxidants. However, its insecticidal family and specifically cypermethrin was investigated mainly in regard with degradation pathways in the soil and water compartments.[8,11,12] Recently, a few investigations regarding pesticides' ozonolysis in aqueous solution (e.g., cypermethrin ozonation) have been published.[13,14] However, these investigations involved an excessive amount of ozone in solution without detailing degradation products.

Ozone is the most common atmospheric oxidant (outdoors and indoors) and is available both during daytime and nighttime.[15] It is especially reactive toward unsaturated hydrocarbons and hence can play a significant role in their degradation both in natural and polluted regions.[15] Heterogeneous oxidation of few other pyrethroids and their analogues by gaseous ozone were investigated by Ruzo et al.[16] This study, which was done under extreme ozone concentrations (10^{18} molecule cm^{-3}) and for a very short exposure times (∼1 min), has shown that the dihalovinyl analogues may yield epoxides of the parent molecules and aldehydes replacing the alkene moiety. In addition, their results imply that in the case of cypermethrin, phosgene (which is a nerve gas) may be produced. However, to the best

* To whom correspondence should be addressed. E-mail: yaeld@tx.technion.ac.il. Phone: (972) 4-829-5899. Fax: (972) 4-822-8898.

10.1021/jp072937t CCC: $37.00
Published on Web 07/19/2007

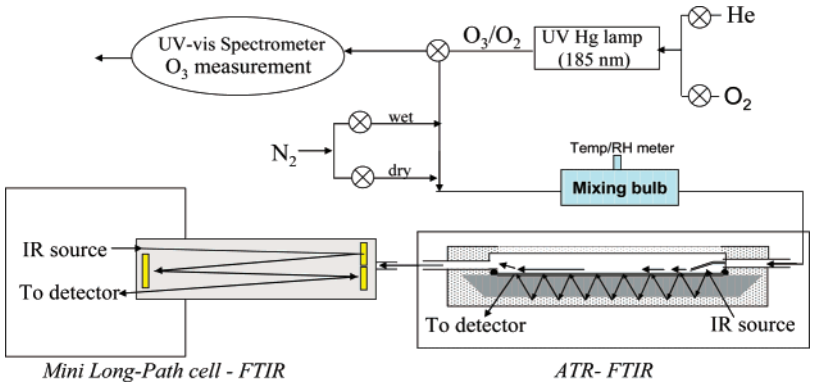

Figure 1. The experimental setup scheme: flow through ATR long path (LP) FTIR.

of our knowledge, the heterogeneous oxidation of cypermethrin by gaseous ozone has not been studied yet.

Laboratory studies directed at atmospheric degradation processes of pesticides are still limited. Most of these studies have focused on photodegradation and OH radicals' reactions of pesticides in the gas phase (using volatile analogues, high volume chambers, or elevated temperature experiments)[17,18] or adsorbed upon aerosols.[19−22]

In the present study, the oxidation of thin film of cypermethrin by gaseous ozone was investigated using a novel apparatus (Figure 1), coupling long-path IR cell and attenuated total reflectance (ATR)-FTIR (from now on LP-ATR-FTIR), for real-time and simultaneous monitoring of both the condensed and gas phases. The use of LP-ATR-FTIR enables us to monitor in a nonintrusive way the heterogeneous ozonolysis of the cypermethrin film and the production of surface and gas-phase products. Reaction rate constants at different ozone concentrations and at low and high relative humidity conditions were obtained. Identification of the reaction products was achieved by both spectral and classic analysis tools (e.g., GC/HPLC-MS). The continuous spectral monitoring enabled us to closely follow the reaction progress and to better predict kinetics and to postulate reaction mechanisms. Atmospheric implications are also discussed.

2. Experimental Section

Experimental Setup. A schematic diagram of the experimental flow through LP-ATR-FTIR setup is shown in Figure 1. The system consists of a 45° horizontal ZnSe ATR crystal (7.5 × 0.8 cm, 10 reflections; HATRPlus by Pike Technologies Inc.), which is placed in a flow-through homemade stainless steel chamber. Metallic surfaces in the chamber and in the LP cell are coated with halocarbon wax, and the tubing is Teflon to minimize ozone loss. The ATR instrument is attached to a Bruker Tensor 27 FTIR with a DTGS detector (spectral range of 6000−350 cm^{-1}). Gas-phase species (including gaseous products) are detected downstream in a small volume long-path IR cell (Infrared Analysis Inc., model 6.2V; 0.5 L with variable path length up to 6 m), based on white cell optics.[23] A high-resolution FTIR (Bruker Vertex 70) with mercury−cadmium−telluride detector is used for gas phase analysis (spectral range of 5000−600 cm^{-1}).

Experimental Procedures. In a typical experiment, ozone was generated by irradiating a dry flow of O_2 and He (both >99.999%, Maxima) with a low-pressure mercury lamp emitting at 185 and 254 nm (Jelight Inc., double bore 78−2046) and then was measured based on absorbance at 254 nm ($\sigma = 1.15 \times 10^{-17}$ cm^2 $molecule^{-1}$ and a path length of 10 cm) using UV−vis spectrometer (Milton Roy Inc., Spectronic 601). Ozone concentration was controlled by varying the exposure of the O_2 to the UV light using an adjustable opaque sheath cover on the lamp and by changing the mixing ratios between the O_2 and He. When the desired concentration was reached, the ozone flow was diverted to the experiment cell. Dilution of nitrogen was added when needed ($[O_3] < 10^{14}$ molecule cm^{-3}) before ozone introduction into the cell (via a mixing cell, $V = 250$ cm^3). Relative humidity (RH) and the temperature of the gas flow was monitored in the mixing cell using AHLBORN Alemo 2390−3 instrument. An ATR background reading was taken on a clean crystal before cypermethrin deposition. A 100 μL sample of 2 mM solution of α-cypermethrin (Riedel-de-Haën, analytical standard) in chloroform (BioLab, analytical reagent) was deposited directly on the ATR crystal. The solvent allowed to evaporate for 5 min before placing the crystal back into the ATR/FTIR holder (complete removal of the solvent was confirmed by ATR spectra). Then, the ATR flow through chamber was sealed. Spectral measurements started simultaneously with diverting the ozone flow to the ATR chamber. The infrared absorbance spectra averaged 32 scans per each spectrum with a resolution of 2 cm^{-1} for condensed phase and 1 cm^{-1} for the gas-phase analysis over a spectral detection range of 4000−600 cm^{-1}. Background for the gas cell was taken under dry nitrogen flow and averaging 64 scans.

Over the spectral range of interest, 600−4000 cm^{-1}, the penetration depth of the evanescent wave into the ATR surrounding in the present experimental system is calculated to be between 1.9 and 0.29 μm, respectively.[24]

Reaction rate constants that were measured for ozone levels range between $10^{11}-10^{15}$ molecule cm^{-3} (30 ppb−60 ppm) at low (∼7% RH) and high-relative humidity (80−90%) conditions. Humidification was obtained by bubbling dry nitrogen gas through DI water (18.2 MΩ water, Millipore).

GC/GC-MS and HPLC-MS Products Analysis. In addition to spectroscopic analysis, the residue of the cypermethrin film was also analyzed by GC-MS and HPLC-MS. Such analysis was done for the verification and identification of observed products on the FTIR instruments. GC-MS (HP 6890 GC with MS detector HP 5973) analysis was done using a capillary column (model number, HP 19091M-433) HP-5 Trace Analysis (5% PH ME Siloxan); 30 m; 250 μm i.d.; film thickness 0.25 μm using a temperature gradient between 50 and 310 °C at a rate of 10 °C/min and an injector temperature of 250 °C. HPLC-MS analysis method used Kromasil 100 C-8 column, mobile phase of 80−20% acetonitrile and water, respectively, and a flow rate of 1.5 mL/min. The analysis was conducted at ambient temperature with an injected volume of 20 μL. The detection was done with a HPLC Agilent 1100 UV detector at 235 nm and a Waters LCT Premier MS detector.

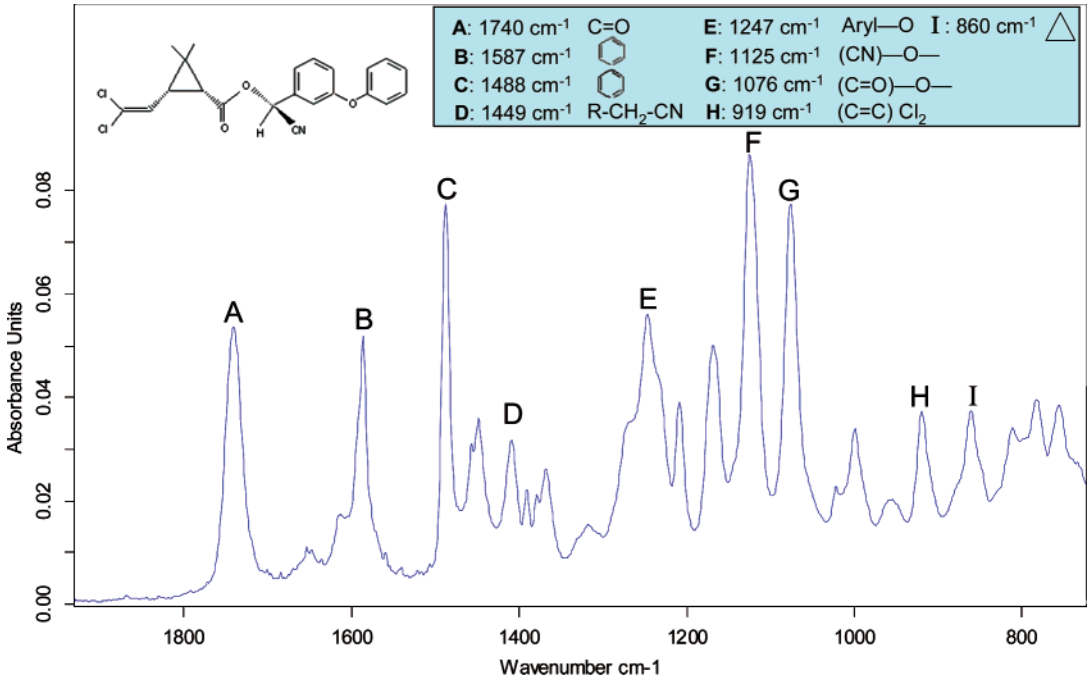

Figure 2. ATR-FTIR spectrum of a thin film of unoxidized cypermethrin at the spectral signature region of the molecule at 1800 and 600 cm^{-1}.

Atomic Force Microscopy (AFM) Imaging. Samples of clean ZnSe crystal and cypermethrin thin films before and after oxidation were imaged by JPK-NanoWizard II AFM, using 3 μm × 3 μm peizoscanner. Imaging was carried out with 10 nm wide-legged silicon cantilever (spring constant of 0.4 N/m) in contact mode.

3. Results and Discussion

In the following, we will discuss the results of cypermethrin oxidation with ozone under different concentrations and different relative humidity conditions. Spectral identification of the reactant and products will be described, followed by a verification analysis using GC-MS and HPLC-MS. Reaction rate constants will be given, as well as a suggested mechanism for the reaction.

Spectral Analysis: Condensed Phase. Figure 2 shows the ATR-FTIR spectrum of cypermethrin, deposited as thin film on the ATR ZnSe crystal. The shown range includes only the fingerprint region, between 1800 and 600 cm^{-1}. In this region, the main absorption bands of cypermethrin are assigned to the carbonyl asymmetric stretching (ν = 1740 cm^{-1}), C═C stretching of the aromatic rings (~1587 and ~1488 cm^{-1}), CH_2 deformation in R—CH_2—CN structure (1448 cm^{-1}) and the (C═O)—O— stretching (1076 cm^{-1}).[25] The band at 1247 cm^{-1}, caused by aryl—O of diphenyl ether, involves aryl—O stretch, out-of-phase C—O—C stretching and ring vibrations.[26] An additional important representing band of the molecule is observed at 1125 cm^{-1} and is related to the C—O stretching of the cyanate group (—O—C≡N).[26] The band at 920 cm^{-1} was assigned to the asymmetric wagging vibrations of the terminal dihalovinyl group, and the band at 860 cm^{-1} was assigned to the deformation vibrations of the cyclopropane ring.[26]

AFM image of a cypermethrin film deposited on a ZnSe substrate (following the same procedure used in the oxidation experiments) is shown in Figure 3. The obtained film (both before and after oxidation) is clearly thinner than the penetration depth of the evanescent wave into the sample at the present experimental system and hence the ATR spectra of the cypermethrin film should resemble its transmission spectra. The observed morphological changes of the film upon oxidation will be discussed later.

The ATR-FTIR spectra recorded during the reaction of cypermethrin with ozone are shown in Figure 4a. As the exposure time to ozone increases, the absorbance at the bands associated with the ester group (1125 and 1076 cm^{-1}) and with the terminal dihalogenvinyl group (920 cm^{-1}) decrease. In parallel, an increase in carbonyl bands (~1740 cm^{-1}) is clearly observed. The carbonyl peak is also broadened during reaction, which may suggest the formation of different carbonyl groups such as aldehydes and carboxylic acids. The observed shifting of the 860 cm^{-1} absorbance band (associated with the cyclopropane ring) may indicate isomerization of the cypermethrin.

Spectroscopic Product Analyses of Condensed Phase. The measured spectra, shown in Figure 4a, are complex and composed of both reactant decrease signals and products increase signals. The spectra interpretation becomes even more challenging as the products of cypermethrin ozonolysis and their specific spectral signatures are unknown. A time-resolved separation between the reactant and products' spectra will enable us to derive kinetic information of the reaction and to help identify its products. However, because of common functional groups between the reactant and products, which overlap in their absorbance bands, such separation is not straightforward. To overcome this obstacle, an isolated absorbance band that is unique to the parent compound has to be identified and can then be used to calculate at each point along the reaction the relative contribution of the parent spectrum to the overall measured spectrum. This allows us to quantitatively subtract that portion and to analyze separately the time evolution of the parent and products spectra (assuming that at a certain time point the complex spectrum is a linear combination of its components). In our case, the band of the dihalovinyl at 920 cm^{-1}, which is unique to the parent compound, was chosen. This peak represents the wag vibration of the double bond, which appears without any overlaps of additional peaks and has no spectral shifting. The band at 1600 cm^{-1}, which is also representative of the unsaturated moiety, was not chosen for this analysis

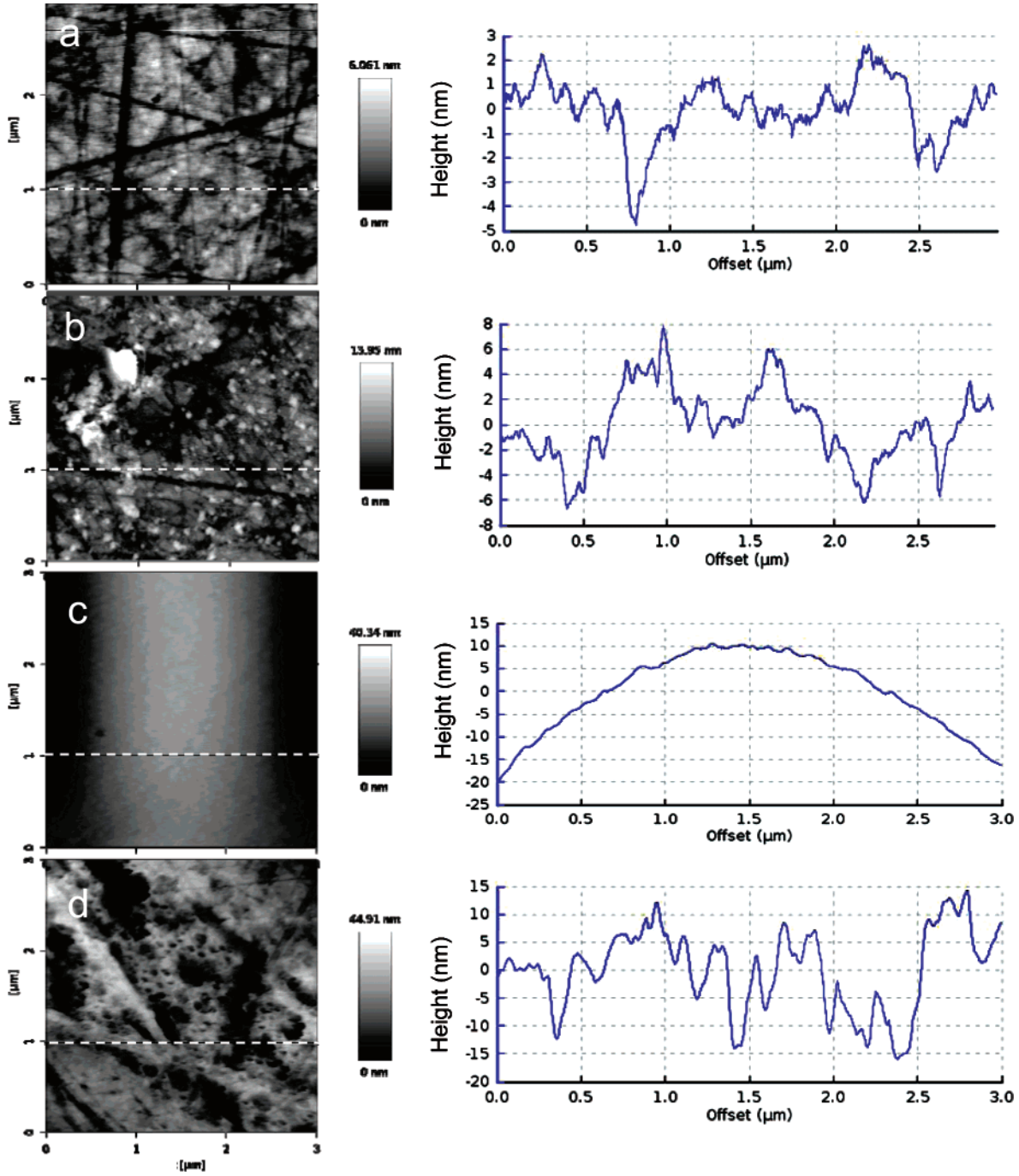

Figure 3. AFM images of clean ZnSe crystal (a), cypermethrin thin film deposited on ZnSe crystal before oxidation (b), and cypermethrin film on ZnSe crystal after ozone exposure (see text) uniform area (c) and irregular area (d). Cross-sectional profiles measured along dashed white lines shown in the images are presented on the right.

because of its obscuration by the aromatic rings stretching band around 1587 cm^{-1}.

At every time step, the relative amount of the cypermethrin spectrum (calculated based on the 920 cm^{-1} band) was subtracted from the specific time step spectrum. The resulting subtracted spectra were obtained using the following eq:

$$S^t_{sub} = S^t_{measured} - \frac{A^t_\nu}{A^{t=0}_\nu} x S^{t=0}_{cyper} \quad (1)$$

where, S^t_{sub} is the subtracted spectrum at time $= t$, $S^t_{measured}$ is the measured spectrum at time $= t$, $A^t_\nu/A^{t=0}_\nu$ is the ratio between the absorbance of the chosen band (920 cm^{-1}) at time t and its absorbance at time zero (before ozone exposure), and $S^{t=0}_{cyper}$ is the spectrum of cypermethrin at time zero (i.e., unreacted cypermethrin). The resulting subtracted spectra are shown in Figure 4b, which actually extracts the increasing peaks in our system. The identified increasing bands, which represent the product's signals, are around 1740 cm^{-1} (aldehydes, ketones, and carboxylic acids carbonyl bond), 1587 cm^{-1} (stretching vibration of aromatic rings), 1488 cm^{-1} (diphenyl ether vibration), and 1448 cm^{-1} ($R-CH_2-CN$). The spectral range between 1400 and 1000 cm^{-1} shows significant overlap between several absorbance bands. This area includes a very broad peak that may be (in part) the result of dimers. The subtraction procedure allowed the extraction of the overall product's spectra and showed that most of the functional groups in the formed

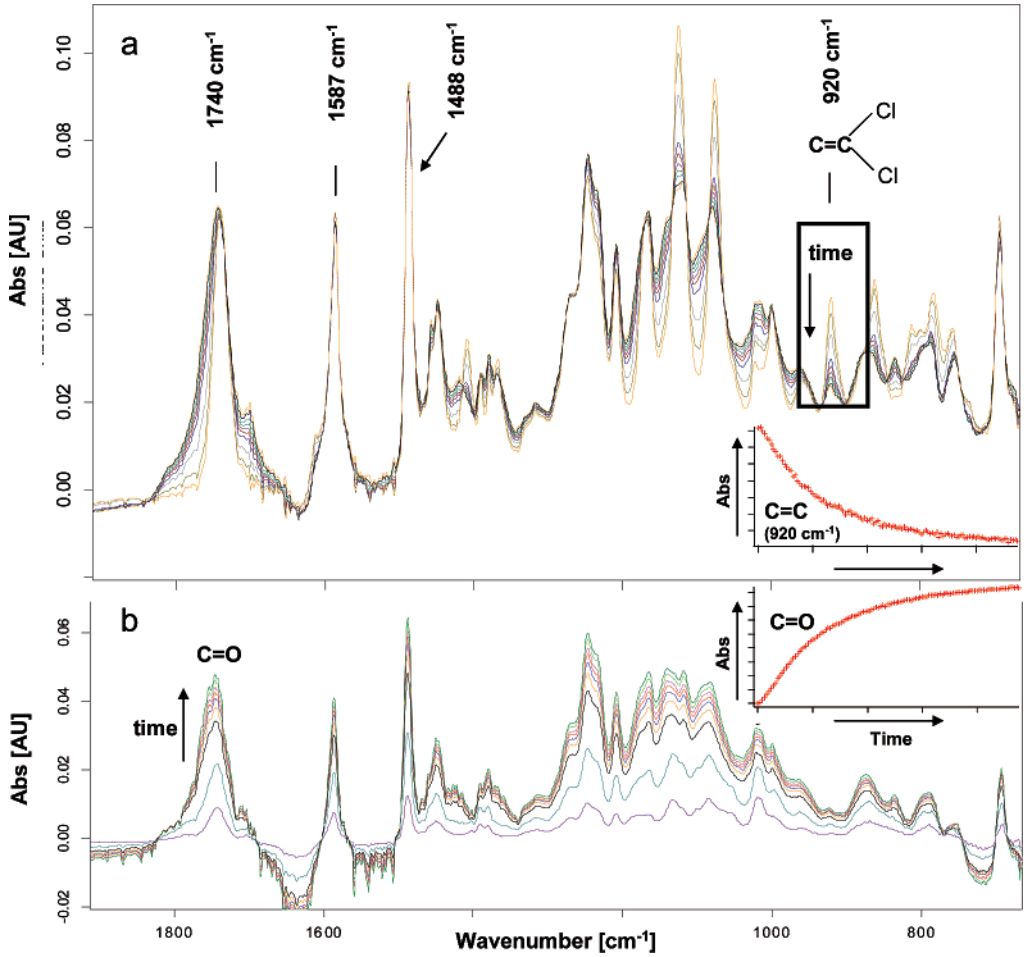

Figure 4. (a) ATR-FTIR spectra recorded during the oxidation of cypermethrin by gaseous ozone. The decrease of the 920 cm^{-1} band (wagging of the dihalovinyl group) along the reaction is shown in the insert. (b) The temporal subtracted spectra representing absorbance due to surface products only. The increase in absorbance at the carbonyl band during reaction, which is clearly revealed in the substracted spectra, is shown in the insert.

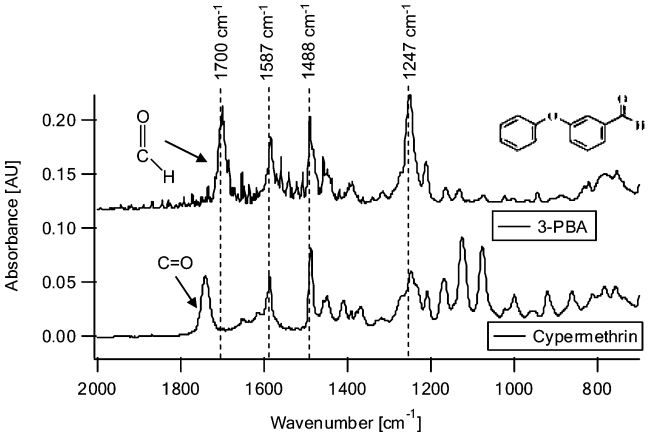

Figure 5. ATR-FTIR spectrum of the surface product identified by the GC-MS 3-phenoxybenzaldehyde (3-PBA).

products are as in the mother material. The main additions to the system are the carbonyl functional groups. The broadness of the obtained absorbance band around 1740 cm^{-1} does support that both aldehydes and carboxylic acids are among the reaction products.

Chromatographic Product Analyses of Condensed Phase. The data interpretation obtained from the ATR infrared spectral analysis suggests the formation of products that contain aromatic rings and carbonyl functional groups that belong to either aldehydes or carboxylic acids. Complimentary analyses of GC-MS and HPLC-MS were performed on the residual film after reaction (the film was extracted from the ATR with 5 mL chloroform or ethanol). For comparison, a film before reaction was also extracted and analyzed. GC-MS analysis has identified the following products: 3-phenoxybenzaldehyde (3-PBA) (product no. 5 in Scheme 1), 6,11-dihydroxy-3-methoxy-1-methyl-12H-benzo[b]xanthen-12-one (DMMB) (product no. 7 in Scheme 1), and 2-cyclopenten-1-one,3-methyl- (product no. 8 in Scheme 1). 3-PBA is one of the known products of the hydrolysis and photolysis reaction of cypermethrin.[11,12] The ATR spectrum of this product, generated using 3-PBA standard (ACROS, 97% purity), indeed agrees with the spectral results, as shown in Figure 5. The 3-PBA representative bands correspond well with the temporal spectral change obtained during reaction, as was shown in Figure 4b, causing an increase in the 1700 cm^{-1} (broadening of the carbonyl band) and at the 1587, 1488, and 1247 cm^{-1} bands. 3-PBA is known to be a minor product relative to 3-phenoxybenzoic acid in hydrolysis and photolysis reactions of cypermethrin. Although the latter was not detected in our GC analysis, which was carried without derivatization and hence is expected to show low sensitivity toward carboxylic acids, the spectral data does indicate the formation of a product with carboxylic acid functional group (the increase and the broadening of the 1740 peak on both sides, as shown in Figure 4). The absorption spectrum of product no. 8 (not shown)

SCHEME 1: Suggested Mechanism for the Heterogeneous Reaction of Cypermethrin with Ozone

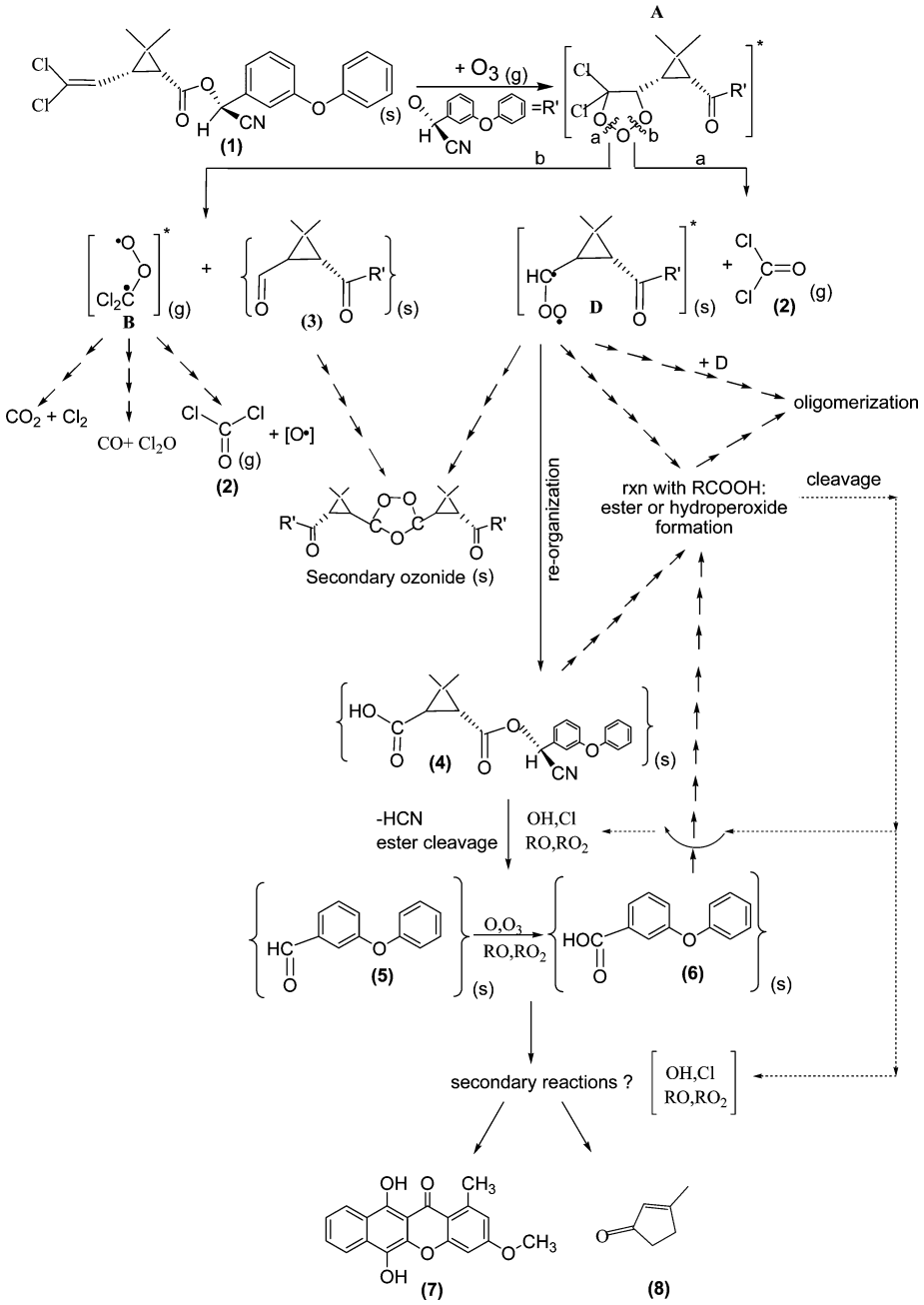

overlaps with other observed peaks and seems to contribute also to the broad absorbance band observed between 1100 and 1400 cm^{-1}.

HPLC analysis also identified several reaction products (including 3-PBA). Although not all were identified, their fast eluation time indicated that these products are more polar than the parent molecule. HPLC analysis has also identified products with a larger molecular mass than cypermethrin (572 versus 416 m/Z), suggesting the formation of secondary ozonide by the reaction of stabilized Criegee intermediates and the aldehyde or acid products[15,27,28] or the formation of oligomers (as partly inferred by the formation of product no. 7, Scheme 1) Furthermore, trans- and cis- secondary ozonides are also expected to show absorption bands around 1320 and 830 cm^{-1}, respectively,[27] which were observed with a small increase in our system. The high-mass product observed by HPLC was the only surface product containing chlorine atoms, indicating that upon ozonolysis of the double bond, most of the chlorine atoms wind up in the gas phase, either as phosgene or as chlorine gas (Cl_2 and Cl_2O), as shown in Scheme 1.

AFM Analysis. In parallel to the chemical changes of the surface upon oxidation (as indicated by the ATR spectroscopy and the chromatography), AFM imaging indicates significant morphological changes (Figure 3b−d). The original cypermethrin film deposited upon the ZnSe crystal formed a thin layer, about 10−15 nm thick (Figure 3b), which still allows us to see the pattern of the crystal beneath (i.e., the crystal lines can be seen, although less clear). After oxidation, the film's morphology changes to form a coating on the crystal with smooth areas of up to about 40 nm in height obscuring the crystal totally (Figure 3c), suggesting that a different coating material has emerged. These smooth areas are dotted by irregular rough areas that are revealing the crystal again in some spots (Figure 3d). This new coating and surface morphology may be the result of secondary surface reactions (yielding secondary ozonides, peroxides, and even oligomers, see Scheme 1) or be

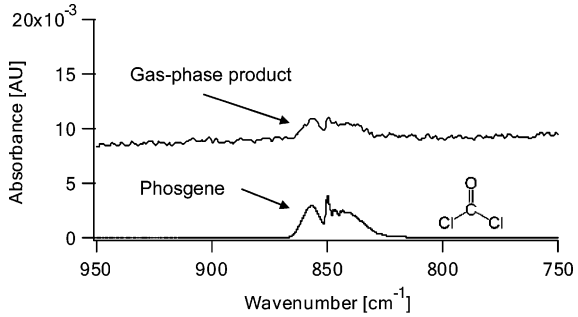

Figure 6. Gas-phase IR spectrum showing the gaseous product found in our experimental system (top) and a reference spectrum of phosgene gas (bottom) (PNNL IR spectra library).

caused by clustering of primary products, such as aldehydes or carboxylic acids that built these aggregates.

Reaction Product: Gas Phase. Gas phase was monitored continuously downstream of the oxidation reactor using mini-LP IR cell (Figure 1) for the detection of gaseous products. Because of the dilution by the carrier gases in these flow through experiments, only a very weak signal of emerged products was seen that were hard to quantify. Hence, we have conducted separate batch experiments of the oxidation reaction of cypermethrin with ozone. In these experiments, two carrier glasses containing a thin film of cypermethrin were inserted into the LP IR cell and placed outside of the path of the IR beam. Following a background scan under a flow of nitrogen gas, ozone was introduced to the cell (flowing through with the gas phase continuously monitored). When reaching a constant level of ozone inside the cell, it was sealed and the monitoring of reaction was continued on the static gas mixture inside the cell. Figure 6 shows the gaseous phase spectra of the emerging product observed during the reaction (~850 cm^{-1}), which fits very well with a phosgene reference spectrum (IR spectral library, *Pacific North National Laboratory*). Phosgene is a highly toxic gas, used as a warfare nerve agent in World War I that is also known to be carcinogenic. In addition to phosgene, qualitative evidence for the formation of gaseous molecular chlorine was obtained by purging the headspace of the cell at the end of the experiment via a *N*,*N*-diethyl-*p*-phenylene-diamine solution, which changes its color in the presence of dissolved chlorine (HACH, test kit for total chlorine model CN-66).

Ozonolysis Kinetics. The time-evolution spectra shown in Figure 4a were recorded under ozone concentration of 4 ppm. Following the subtraction procedure discussed above, changes in absorbance of the various functional groups during oxidation were evaluated based on the corresponding peak area. The obtained exponential fits and rate coefficients for these changes (at this particular ozone concentration) are shown in Figure 7.

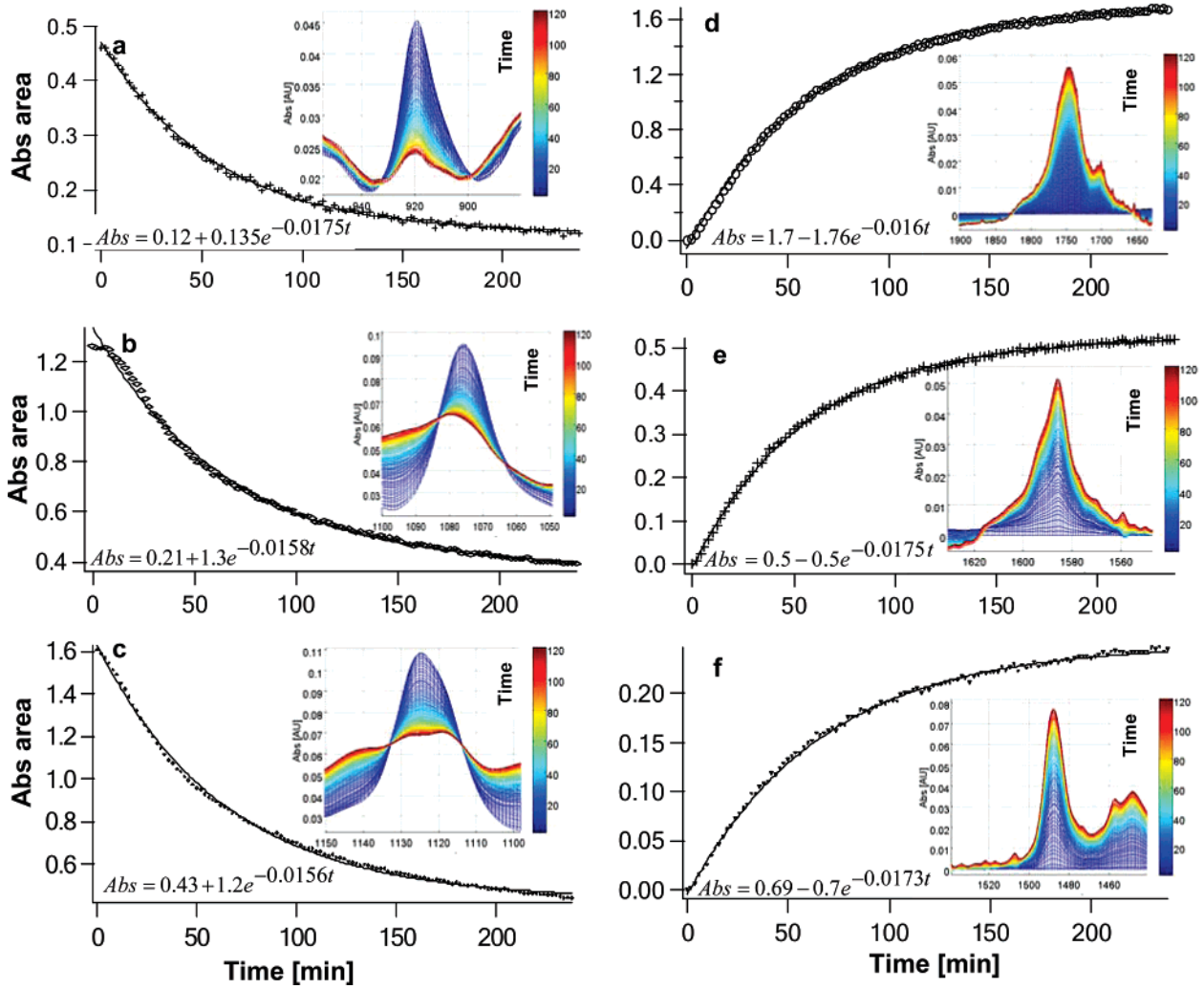

Figure 7. Temporal changes in the infrared absorbance spectra showed in Figure 4a (4 ppm O_3) focusing on several spectral bands: (a) 920, (b) 1076, (c) 1125, (d) 1740, (e) 1587, and (f) 1488 cm^{-1}. The absorbances shown were calculated based on peak area integration. For each band, the solid line represents exponential fit of the data given by $A(t) = A_0 + Be^{-kt}$, where the sum of A_0 and B is the absorbance at time zero, and k is the pseudo-first-order rate coefficient. In the insets, changes of the specific peaks with time are shown.

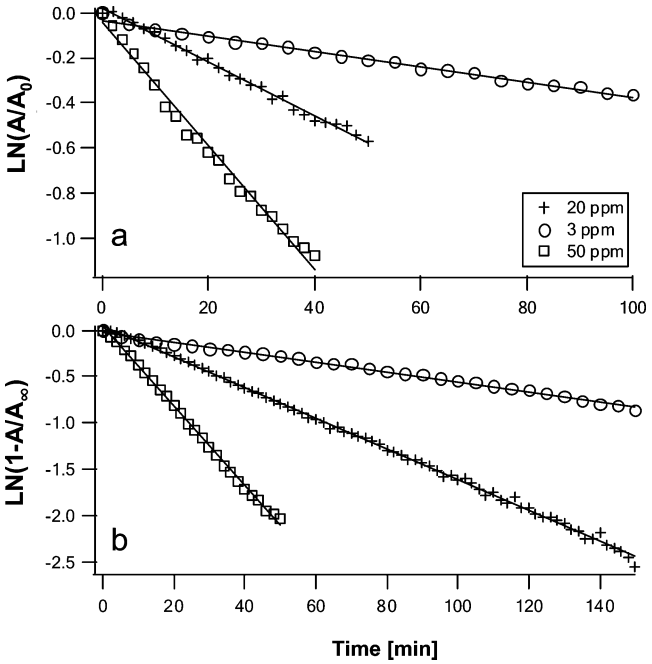

Figure 8. (a) Representative cypermethrin decay plots based on absorbance at 920 cm^{-1} during exposure to gaseous ozone at concentrations of: 3 ppm (O), 20 ppm (+), and 50 ppm (□); (b) representative temporal buildup plots of the carbonyl group (1740 cm^{-1}) during oxidation with ozone at concentrations of 3 ppm (O), 20 ppm (+), and 50 ppm (□). Similar trends were observed at lower ozone concentrations (data not shown for convenience reason only).

The loss of the dihalovinyl group (920 cm^{-1}) and the ether groups (1076 and 1125 cm^{-1}) are shown in Figure 7a−c, respectively. The buildup of the carbonyl group (1740 cm^{-1}), the product's aromatic rings (1587 cm^{-1}), and the diphenyl ether (1488 cm^{-1}) are shown in Figure 7 d−f, respectively. The experimental data show good fit to an exponential decay process. Blank experiments of thin film cypermethrin under nitrogen and oxygen flows, at the same experimental conditions did not show any spectral change with time.

As shown in Figure 7, the observed rate constants for the loss of cypermethrin and the growth of the products are very similar. The small difference between the loss rate constants of the esters (1076 and 1125 cm^{-1} bands) and of the terminal vinyl band (920 cm^{-1}) cannot be proven to be significant (not enough data) and may also be the result of an artifact caused by the superimposing of the 1076 and 1125 cm^{-1} bands with a broad band as shown in Figure 4b.

The loss of cypermethrin upon exposure to ozone was monitored, as a function of time and gaseous ozone levels, using the change in the absorbance area of the terminal dihalovinyl group at 920 cm^{-1}. Figure 8a shows the linear correlation between the logarithm of absorbance area and time. The linearity of the plots demonstrates that the reaction can be considered as first order with respect to cypermethrin. The slopes of the linear least-squares fits of these plots (all obtained $r^2 > 0.95$) were used to determine the observed pseudo-first-order rate coefficients, k_I, using eq 2.

$$\ln\left(\frac{[C]}{[C]_0}\right) = -k_I t \tag{2}$$

where $[C]_0$ and $[C]$are the cypermethrin concentration at time zero and time t, respectively, k_I is the first-order reaction rate constant, and t is the reaction time interval.

Because the absorbance is linearly proportional to the concentration (according to Beer−Lambert law), the ratio between concentrations equals the ratio between the absorbances. Hence, drawing the absorbances' ratio as a function of time will yield the same observed k_I for the oxidation reaction of cypermethrin with ozone.

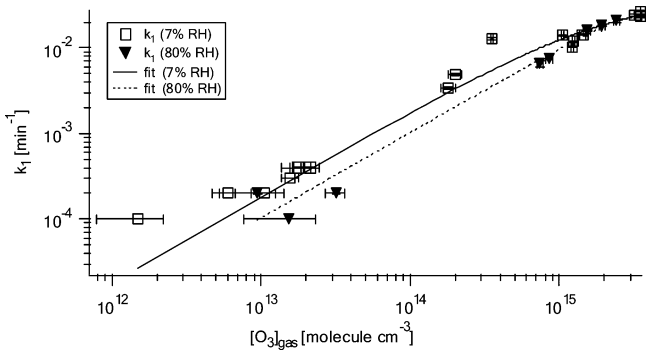

Figure 9. Pseudo-first-order reaction rate constants for the reaction of cypermethrin with ozone at low RH, ∼7%, (□) and high RH, ∼80%, (▼).

As product's buildup data was fitted by an exponential growth to a maximum (eq 3 and Figure 7d−f), the first-order rate coefficient for their formation was obtained from the linear plots shown in Figure 8b using eq 4

$$[C] = [C]_\infty \cdot [1 - e^{-k_I t}] \tag{3}$$

$$\ln\left(1 - \frac{[C]}{[C]_\infty}\right) = -k_I t \tag{4}$$

where $[C]_\infty$ is the product concentration at the end of reaction (after reaching the plateau).

Again, because we are dealing with the concentration ratios, the corresponding absorbance ratios can be used, as plotted in Figure 8b.

The observed k_I values, extracted from the data fits, as in Figure 8a, at the various ozone concentrations are plotted in Figure 9. Under the present experimental conditions (ozone in excess), the observed pseudo-first-order reaction rate coefficient k_I is the product of the second-order reaction rate constant k_s (k surface) and the surface ozone concentration. The data in Figure 9 fit well with a Langmuir−Hinshelwood surface reaction mechanism, as described by eq 5, indicating that cypermethrin reacts on the surface with adsorbed ozone that is in rapid equilibrium with the gas phase.[29] Furthermore, the good exponential fits shown in Figure 7 strengthen the assumption that the majority of the reaction occurs on the surface, rather than in the bulk.[28]

$$k_I = \frac{k_s[S]K_{O_3}[O_3]_{gas}}{1 + K_{O_3}[O_3]_{gas}} \tag{5}$$

Where k_I [1/min] is the pseudo-first-order reaction rate constant, k_s [cm^2 min^{-1} $molecule^{-1}$] is the second-order surface reaction rate constant, S [molecule cm^{-2}] is the total (maximum) surface density of O_3 adsorption sites, K_{O_3} [cm^3 $molecule^{-1}$] is the ratio between ozone adsorption and desorption rate coefficients, and $[O_3]_{gas}$ is the ozone concentration measured in the gas-phase near the surface [molecule cm^{-3}]. The parameters $k_s[S]$ and K_{O_3} obtained from the data fit are: 0.039 ± 0.007 [min^{-1}] and $(4.7 \pm 1.7) \times 10^{-16}$, respectively. The calculated K_{O_3} for the present system is lower in 1 order of magnitude relative to the K_{O_3} obtained previously in heterogeneous ozonolysis of anthracene film at the air−water interface[30] and of benzo[a]pyrene on solid organic aerosols (Table 1).[31] When

TABLE 1: Comparison between Different Reaction Rate Constants Obtained from the Heterogeneous Reaction of Ozone and Molecules Containing Vinyl Bonds

reaction of O_3 with:	K_{O_3} (cm^3 $molecule^{-1}$)	$k_s \times S$ ($= k_{s,max}{}^{I}$) (sec^{-1})	
cypermethrin on inert substrate (ZnSe)	$(4.7 \pm 1.7) \times 10^{-16}$	0.0007 ± 0.0001	present study
benzo[a]pyrene on azelaic acid aerosols	$(1.2 \pm 0.4) \times 10^{-15}$	0.048 ± 0.008	Kwamena et al., 2004
benzo[a]pyrene on soot	$(2.8 \pm 0.2) \times 10^{-13}$	0.015 ± 0.001	Pöschl et al., 2001
anthracene film on octanol aqueous solution	$(2.5 \pm 0.1) \times 10^{-15}$	0.002 ± 0.0002	Mmereki et al., 2004
vinyl-terminated SAMs	$(2.5 \pm 0.4) \times 10^{-14}$	0.006 ± 0.003	Dubowski et al., 2004

compared to the reaction of O_3 with benzo[a]pyrene on soot[32] and on vinyl-terminated self-assembled monolayers (SAMs),[33] the obtained value is even lower suggesting that ozone binding to cypermethrin film is weaker than to soot and (to a lesser extent) to SAMs. This trend is not surprising considering the presence of radical sites on soot to which ozone is expected to strongly bind and the higher order and density of the SAMs with the double bonds at the interface with gas phase. The obtained maximum surface rate constant (i.e., $k_s[S]$) for cypermethrin ozonolysis is much slower than previously reported rates for the oxidation of benzo[a]pyrene,[31,32] anthracene,[30] and of vinyl-terminated SAMs.[33] The relatively slow oxidation rate of cypermethrin can be explained both by the complexicity of this molecule relative to the molecules already investigated (i.e., steric effects that may cause hindering of reaction sites)[34] and the probable deactivation of the double bond by adjacent chlorine atoms.[35]

Influence of Relative Humidity (RH). Figure 9 shows the observed pseudo-first-order reaction rate coefficients k_I for cypermethrin ozonolysis under low (~7%) and high (~80%) RH. In the latter, the obtained k_I values were somewhat lower than under low RH, but according to the Oneway Anova test, which tests out the difference in means between the two groups, the obtained difference is not significant (P-value = 0.299).

Suggested Oxidation Mechanism. On the basis of the kinetic results and the product identification, together with the theoretical knowledge regarding ozonolysis reactions with unsaturated moieties, a reaction mechanism is postulated as shown in Scheme 1. The following text refers to the product's numbers and the pathways marked on the scheme.

The first process to occur is the formation of primary ozonide on the double bond (A). This ozonide has two decomposing options (a and b), each forming two Criegee intermediates.[15] Pathway "a" forms gaseous phosgene (product 2 in Scheme 1) and a condensed intermediate D that after reorganization will form the carboxylic acid (product 4 in Scheme 1).[27] Intermediate D can also react on the surface with aldehydes or acids to form secondary ozonides or hydroperoxides (via ester formation).[27,36] Cleavage of the latter (which is known to occur in the gas phase) may generate OH and alkoxy radicals.[37] Also, the availability of such radicals and chlorine atoms in this system can lead to the formation of chlorine radicals as well. The formation of such radicals is postulated to cause the ester cleavage and the formation of the identified product (3-PBA). As was mentioned earlier, spectral data support that both aldehyde and carboxylic acid (products 5 and 6, respectively) are present on the surface. Conducting the ozonolysis experiments in the presence of gaseous cyclohexane, which is a known OH scavenger, did not yield any changes in the observed reaction rate, suggesting that the OH formation occurs mainly within the film on the surface (out of the cyclohexane reach) or that other radicals (e.g., chlorine, alkylperoxy and alkoxy radicals) are more dominant. In addition, radical formation can cause chain reactions and can promote oligomerization on the surface. The high mass products identified in the HPLC-MS and the morphological changes observed by the AFM supports this assumption.

Pathway "b" leads to the possible formation of a surface aldehyde (product 3) and a gaseous intermediate B that can be transformed to form CO_2 and Cl_2, Cl_2O and CO, or decompose into phosgene and an oxygen radical. The latter can participate in all the other pathways as mentioned above. A small increase of the CO signal at 2270 cm^{-1} was detected during the static reaction. However, it was not quantified due to interferences by CO_2 absorption. The formation of phosgene was supported by the gas-phase spectra, as shown in Figure 6. Products 7 and 8 (detected by GC-MS) are postulated to form by secondary reactions involving radicals (possibly OH, alkoxy, and Cl radicals) attack on the ester cleavage products and the parent molecule. Previous detection of product 8 as a product during the photo-oxidation reaction of toluene with OH radicals[38] strengthens the assumption of secondary surface reactions involving radicals in the preset system. Products 7 and 8 were not detected previously under the investigation of cypermethrin photolysis or hydrolysis.

Conclusions and Environmental Implications

In this study, we have investigated the heterogeneous reaction of cypermethrin, a widely used pesticide, with ozone. The investigation was carried out via a nonintrusive analysis method of FTIR spectroscopy. The experimental system, conjugated ATR-FTIR and a long path IR cell, was used to monitor simultaneously both the condensed and the gas phases. We have shown that much of the kinetics of both reactant and the yielding products can be extracted solely from the obtained spectra. This analysis can be used as a powerful tool in the investigation of environmental fate of such toxic compounds.

The heterogeneous oxidation of cypermethrin film by ozone fit well with the Langmuir−Hinshlwood mechanism. The fit parameters obtained in the present study indicate that under common atmospheric ozone concentration of 50 ppb, the half-life of cypermethrin due to heterogeneous ozonolysis is about 21 days. Such a life time is of the same order of magnitude as previously reported lifetimes due to hydrolysis and photolysis in natural water.[10−12,39−41] Thus, the oxidation of cypermethrin residue on surfaces by gaseous ozone seems to play an important role in its environmental fate. The film obtained in the laboratory experiments resembles field conditions, because during pesticides application they are sprayed in a mixture of organic solvents, which rapidly evaporates leaving the active ingredient airborne or deposited on different surfaces, which are exposed to the atmosphere. The current experimental system deals only with artificial surface (ZnSe) although different surfaces are expected to influence cypermethrin lifetime and degradation products, as seen in other investigations regarding cypermethrin photochemistry[42,43] or heterogeneous ozonolysis of other organic films.[31] The research of oxidation upon different surfaces is still undergoing and will add necessary data for better understanding of this environmental process.

Although high RH did not seem to play a major role in cypermethrin ozonolysis rate, additional atmospheric oxidants such as OH radicals, are expected to affect its degradation rate and products. The reaction of cypermethrin with OH· is currently under investigation in our laboratory.

In general, the proposed reaction mechanism for the oxidation of cypermethrin by ozone involves both classical alkenes

ozonolysis and secondary chemistry involving radicals chain reactions to form secondary ozonides, ester cleavage products, and possibly oligomers on the surface. These observations show high similarity to the model investigations of oleic acid ozonolysis.[44]

The condensed phase IR spectra show the formation of carbonyl groups and aromatic rings of diphenyl ether supporting the off-line product identification of 3-PBA and products 7 and 8 shown in Scheme 1. 3-PBA (as well as 3-phenoxybenzoic acid) are more polar than the parent molecule and, while released to the environment or after redeposition, may be susceptible to a greater leaching rate in soils, as shown by Kaufman et. al. in 1981[8] and hence to a greater groundwater contamination probability, relative to the parent molecule. 3-PBA is a toxic compound that was recently proven to have also estrogenic activity (interacts with cellular estrogen receptors).[45] Currently, there is little information regarding the degradation of these oxidation products, and hence their environmental persistence and fate is still not fully clear.

AFM results indicate a significant change in surface morphology with possible increase in the surface area following cypermethrin oxidation (Figure 3c,d). These morphological changes (due to possible formation of secondary ozonides, oligomers, or clustering on the surface) may also affect other surface chemistry processes that can occur upon this film, either when deposited on stagnant surfaces or as airborne particle. Interestingly, aggregation phenomena has also been reported previously during the heterogeneous ozonolysis of vinyl-terminated SAMs,[46] suggesting that this may be a more general phenomena during surface oxidation of unsaturated organic films. Formation of such secondary coatings may also affect the hygroscopic properties of the oxidized surface. Interestingly, despite the formation of polar products and increasing surface roughness during the ozonolysis of the cypermethrin films preliminary data (not shown) regarding its water uptake show only little increase following its ozonolysis (similar to the observations during the oxidation of unsaturated SAMs).[46]

The gas-phase IR spectra show the formation of phosgene and possibly also carbon monoxide. Phosgene is a stable gas extremely toxic by even a short term inhalation exposure; when bearing in mind that cypermethrin is also an indoor insecticide, the release of phosgene (which is heavier than air) upon ozonolysis may impose a health hazard. Although the observed formation yield of phosgene from cypermethrin ozonolysis was on the order of only few percents (~6−10%), its occurrence and possible accumulation in poorly ventilated indoor environments does raise the real need for additional knowledge regarding the heterogeneous degradation processes and indoor fate of cypermetrhin and similar indoor insecticides.

Acknowledgment. This research was funded by Marie Currie International Reintegration grant, as part of the sixth framework programme of the European Commission. We also thank the anonymous reviewers for their valuable comments.

References and Notes

(1) Seiber, J. N.; Woodrow, J. E. *Residue Rev.* **1983**, *85*, 217.

(2) Aston, L. S.; Seiber, J. N. *J. Environ. Qual.* **1997**, *26*, 1483.

(3) Chernyak, S. M.; Rice, C. P.; McConnell, L. L. *Mar. Pollut. Bull.* **1996**, *32*, 410.

(4) Majewski, M. S.; McChesney, M. M.; Woodrow, J. E.; Prueger, J. H.; Seiber, J. N. *J. Environ. Qual.* **1995**, *24*, 742.

(5) Seiber, J. N.; Woodrow, J. E. Origin and Fate of Pesticides in Air. In *Eighth International Congress of Pesticide Chemistry*; Ragsdale, N. N., Kearney, P. C., Plimmer, J. R., Eds.; Oxford University Press: New York, 1995.

(6) Wolters, A.; Linnemann, V.; Herbst, M.; Klein, M.; Schaffer, A.; Vereecken, H. *J. Environ. Qual.* **2003**, *32*, 1183.

(7) Wolfe, M. F.; Seiber, J. N. *Occup. Med.: State of the Art Rev.* **1993**, *8*, 561.

(8) Kaufman, D. D.; Russell, B. A.; Helling, C. S.; Kayser, A. J. *J. Agric. Food Chem.* **1981**, *29*, 239.

(9) Jones, D. Environmental Fate of Cypermethrin. In *Environmental Monitoring and Pest Management*; Department of Pesticide Regulation, 1995.

(10) Bacci, E.; Calamari, D.; Gaggi, C.; Vighi, M. *Chemosphere* **1987**, *16*, 1373.

(11) Takahashi, N.; Mikami, N.; Matsuda, T.; Miyamoto, J. *J. Pestic. Sci.* **1985**, *10*, 643.

(12) Takahashi, N.; Mikami, N.; Matsuda, T.; Miyamoto, J. *J. Pestic. Sci.* **1985**, *10*, 629.

(13) Wu, J. G.; Luan, T. G.; Lan, C. Y.; Lo, T. W. H.; Chan, G. Y. S. *Food Control* **2007**, *18*, (466)

(14) Wu, J. G.; Luan, T. G.; Lan, C. Y.; Lo, W. H.; Chan, G. Y. S. *J. Food Eng.* **2007**, *79*, 803.

(15) Finlayson-Pitts, B. J.; Pitts, J. N. *Chemistry of the Lower and Upper Atmosphere*; Academic Press: San Diego, CA, 2000.

(16) Ruzo, L. O.; Kimmel, E. C.; Casida, J. E. *J. Agric. Food Chem.* **1986**, *34*, 937.

(17) Xu, Y. P.; Zhu, T.; Li, S. J. *Prog. Nat. Sci.* **2002**, *12*, 185.

(18) Feigenbrugel, V.; Le Person, A.; Le Calve, S.; Mellouki, A.; Munoz, A.; Wirtz, K. *Environ. Sci. Technol.* **2006**, *40*, 850.

(19) Palm, W.-U.; Elend, M.; Krueger, H. U.; Zetzsch, C. *Environ. Sci. Technol.* **1997**, *31*, 3389.

(20) Palm, W. U.; Millet, M.; Zetzsch, C. *Ecotoxicol. Environ. Saf.* **1998**, *41*, 36

(21) Palm, W. U.; Elend, M.; Kruger, H. U.; Zetzsch, C. *Chemosphere* **1999**, *38*, 1241.

(22) Samsonov, Y. N.; Makarov, V. I. *Bull. Environ. Contam. Toxicol.* **1996**, *56*, 903.

(23) White, J. U. *J. Opt. Soc. Am.* **1942**, *32*, 285.

(24) Harrick, N. J. *Internal Reflection Spectroscopy*; Harrick Publications: New York, 1967.

(25) Armenta, S.; Quintas, G.; Garrigues, S.; de la Guardia, M. *Talanta* **2005**, *67*, 634.

(26) Lin-Vien, D.; Colthup, N. B.; Fateley, W. G.; Grasselli, J. G. *The handbook of Infrared and Raman Frequencies of Organic Molecules*; Academic Press: London, 1991.

(27) Bailey, P. S. *Ozonation in Organic Chemistry*; Academic Press: New York, 1978; Vol. 1.

(28) Hearn, J. D.; Lovett, A. J.; Smith, G. D. *Phys. Chem. Chem. Phys.* **2005**, *7*, 501.

(29) Ammann, M.; Poschl, U.; Rudich, Y. *Phys. Chem. Chem. Phys.* **2003**, *5*, 351.

(30) Mmereki, B. T.; Donaldson, D. J.; Gilman, J. B.; Eliason, T. L.; Vaida, V. *Atmos. Environ.* **2004**, *38*, 6091.

(31) Kwamena, N.; Thornton, J.; Abbatt, J. *J. Phys. Chem. A* **2004**, *108*, 11626.

(32) Poschel, U.; Letzel, T.; Schauer, C.; Niessner, R. *J. Phys. Chem. A* **2001**, *105*, 4029.

(33) Dubowski, Y.; Vieceli, J.; Tobias, D. J.; Gomez, A.; Lin, A.; Nizkorodov, S. A.; McIntire, T. M.; Finlayson-Pitts, B. J. *J. Phys. Chem. A* **2004**, *108*, 10473.

(34) Ruzo, L. O.; Krishnamurthy, V. V.; Casida, J. E.; Gohre, K. *J. Agric. Food Chem.* **1987**, *35*, 879.

(35) Atkinson, R.; Carer, W. L. *Chem. Rev.* **1984**, *84*, 437.

(36) Hung, H. M.; Katrib, Y.; Martin, S. T. *J. Phys. Chem. A* **2005**, *109*, 4517.

(37) Paulson, S. E.; Orzechowskaa, G. E. *Atmos. Environ.* **2002**, *36*, 571.

(38) Hamiltona, J. F.; Webba, P. J.; Lewisa, A. C.; Reviejo, M. M. *Atmos. Environ.* **2005**, *39*, 7263−7275.

(39) Class, T. J. *Int. J. Environ. Anal. Chem.* **1992**, *49*, 189.

(40) *The Agrochemicals Handbook*, Third Edition; Kidd, H., James, D. R., Eds.; Royal Society of Chemistry Information Services: Cambridge, U.K., 1991.

(41) Walker, M. H.; Keith, L. H. *EPA's Pesticide Fact Sheet Database*; Lewis Publishers: Chelsea, MI, 1992.

(42) Katagi, T. *J. Agric. Food Chem.* **1991**, *39*, 1351.

(43) Katagi, T. *J. Agric. Food Chem.* **1992**, *40*, 1269.

(44) Zahardis, J.; Petrucci, G. A. *Atmos. Chem. Phys.* **2007**, *7*, 1237−1274.

(45) McCarthy, A. R.; Thomson, B. M.; Shaw, I. C.; Abella, A. D. *J. Environ. Monit.* **2006**, *8*, 197.

(46) McIntire, T. M.; Gaspar, D. J.; Jaitly, N.; Dubowski, Y.; Li, Q.; Penner, R. M.; Finlayson-Pitts, B. J. *Phys. Chem. Chem. Phys. 7* **2005**, *7*, 3605.